3D CTA IMAGE SEGMENTATION WITH A GENERALIZED CYLINDER-BASED TREE MODEL

Julien Mille

Université de Lyon, CNRS
Université Lyon 1, LIRIS, UMR5205
F-69622, France
julien.mille@liris.cnrs.fr

Laurent D. Cohen

CEREMADE, UMR CNRS 7534
Université Paris Dauphine
F-75775, France
cohen@ceremade.dauphine.fr

ABSTRACT

The proposed model is devoted to the segmentation and reconstruction of 3D vascular trees [1]. We rely on an explicit representation of a deformable tree, where topological relationships between segments are modeled. This allows easy posterior interactions and quantitative analysis, such as measuring diameters or lengths of vessels. Starting from a unique user-provided root point, an initial tree is built with a technique relying on minimal paths. Within the constructed tree, the central curve of each segment and an associated variable radius function evolve in order to satisfy a region homogeneity criterion. We present results obtained on 3D CTA images of the carotid bifurcation.

Index Terms— Generalized cylinder, tree, segmentation, CTA, vessel

1. INTRODUCTION

The recovery of branching structures, especially vascular trees in MRA, CTA or retinal images, has been an extensively studied subject [1, 2, 3]. In this context, a major concern lies in the extraction of centerlines and thicknesses of significant branches, which make up relevant data for posterior clinical study. Specifically, a tree modeling algorithm should be able to handle imaging issues like great variability in length and thickness of segments. Many methods dealing with centerlines extraction like [3] make sequential tracking of segments, in the sense that the whole final tree structure is propagated from one or several seed location(s). Given a search window, points are consecutively added to segments regarding intensity features. The difficulty lies in the implementation of techniques dealing with junctions, whether current segment should be split or not. Moreover, topological relationships between segments are not necessarily represented.

[1]This work was supported by ANR grant MESANGE ANR-08-BLAN-0198

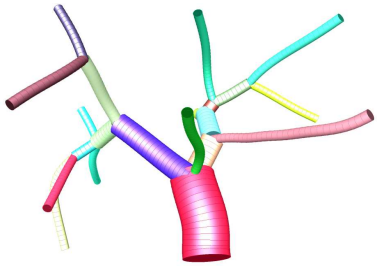

Fig. 1. 3D tree structure, in which segments are generalized cylinders

We propose a novel deformable tree model based on generalized cylinders (see fig. 1). It is slightly related to the work in [2, 4], as minimal paths [5] intervene in the construction of centerlines. However, our approach differs from those in the sense that the initial tree is built by back-propagation from endpoints to the user-provided root point. This avoids to implement decision mechanisms to handle junction points, which may rely on sensitive thresholds. The obtained structure explicitly represents topological relationships between segments (the parent segment and children are known for a given segment). Then, each segment is endowed with a deformable generalized cylinder defined by a central curve and a radius function, which both evolve with respect to a variational homogeneity criterion similar to [6]. The evolution of the deformable tree lies on the simultaneous evolution of all generalized cylinders. The esimated tree volume is voxelized and refined using an implicit active surface. We finally present results obtained on 3D CTA images of the carotid bifurcation, in which segmentation is performed on vessel lumens and compared to ground truth.

2. INTENSITY ENHANCEMENT

Due to the injection of contrast agent before imaging, the vessel lumen is brighter than neighboring structures like muscles and fat. It remains however darker than bone. As a prepro-

cessing step before building the deformable tree, we enhance intensities around a reference intensity I_{ref}, making the reasonable assumption that intensity within the lumen follows a Gaussian distribution. The transformation is implemented through a look-up table computed with

$$I_{\text{output}} = \exp\left(\frac{(I_{\text{input}} - I_{\text{ref}})^2}{2\sigma^2}\right)$$

The reference intensity I_{ref} is chosen as the mean intensity in a small neighborhood around one of the provided initial points. The standard deviation is set to $\sigma = 20$. In the remainder of the paper, I corresponds to the enhanced intensity.

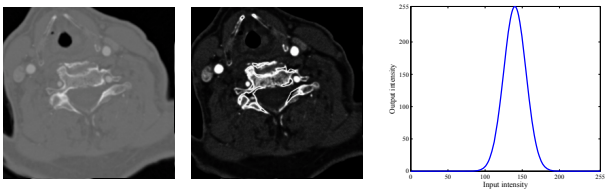

Fig. 2. Vessel intensity enhancement : initial image (left), enhanced image (center), Gaussian look-up table (right)

3. BUILDING THE INITIAL TREE WITH MINIMAL PATHS

The minimal path approach by Cohen and Kimmel [5] aims at finding curves of minimal length in a Riemannian space endowed with an isotropic metric. The length of path $\mathcal{C}$ is:

$$L[\mathcal{C}] = \int_0^1 w + P(\mathcal{C}(s))ds \qquad (1)$$

where s is the arc length and w is a regularization constant. Potential P, which defines the isotropic metric, is either intensity-based or gradient-based, depending on the application. The minimal path approach determines a global minimum of the energy, given two fixed endpoints $\mathbf{x}_0$ and $\mathbf{x}_1$. First, the minimal action map $\mathcal{U}_0$, which corresponds to the minimal cost integrated along a path starting at $\mathbf{x}_0$ and ending at $\mathbf{x}$, is computed by the Fast Marching method. Then, the geodesic path γ linking point $\mathbf{x}_1$ to $\mathbf{x}_0$ is found by back-propagation on $\mathcal{U}_0$, starting from $\mathbf{x}_1$ until $\mathbf{x}_0$ is reached.

As we seek for bright vessels in our application, we use an intensity-based potential computed on the enhanced image. Vessels endpoints are provided in the test datasets. The following potential function achieves a quickly increasing penalty in dark areas:

$$P(\mathbf{x}) = \frac{1}{2} + \frac{\arctan\left(\lambda(1 - 2I(\mathbf{x}))\right)}{2\arctan\lambda} \qquad \in [0,1]$$

where $\lambda > 1$ is the chosen slope. The action map is propagated from the most relevant root location, which is one of the provided endpoints. Gradient descent of the action map is subsequently performed starting from the other endpoints. Instead of applying independent back-trackings, we check for the presence of an already traced path at each gradient descent step. Hence, a structure of connected paths is built. Portions of paths between two junctions (or between a junction and an endpoint) become tree segments.

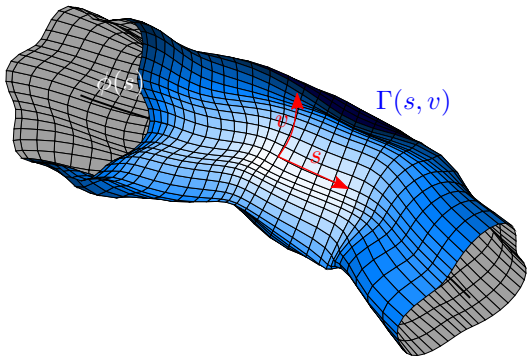

Fig. 3. Deformable generalized cylinder: radius varies both along and around the axis

4. DEFORMABLE GENERALIZED CYLINDER FOR TUBULAR STRUCTURES REPRESENTATION

Each tree segment is endowed with a generalized cylinder, which represents the vessel centerline and radius. Let $\phi : [0,1] \rightarrow \mathbb{R}^3$ be the curved axis, parameterized by arc-length s, and $\mathcal{R} : [0,1] \times [0,2\pi] \rightarrow \mathbb{R}^+$ the radius function. Let $\mathbf{T}$, $\mathbf{N}$ and $\mathbf{B}$ be the tangent, normal and binormal vectors of curve ϕ. Frame $\{\mathbf{T}, \mathbf{N}, \mathbf{B}\}$ defines an orthogonal coordinate system sweeping along the curve. It is used to build varying cross-sections orthogonal to the curve's local direction. Hence, the surface position vector is defined as follows:

$$\Gamma(s,v) = \phi(s) + \mathcal{R}(s,v)(\cos v\mathbf{N} + \sin v\mathbf{B})$$

where parameters s and v sweep along and around the cylinder, respectively (see fig. 3). As stated in [7], defining the surface in this way yields an undesirable twisting effect on the cylinder. Actually, we compute corrected normal and binormal vectors (denoted with *) following [8]:

$$\begin{aligned}\mathbf{N}^*(s+\Delta s) &= \frac{\mathbf{N}^*(s) - \langle \mathbf{N}^*(s), \mathbf{T}(s+\Delta s)\rangle\, \mathbf{T}(s+\Delta s)}{\|\mathbf{N}^*(s) - \langle \mathbf{N}^*(s), \mathbf{T}(s+\Delta s)\rangle\, \mathbf{T}(s+\Delta s)\|} \\ \mathbf{B}^*(s+\Delta s) &= \mathbf{T}^*(s+\Delta s) \times \mathbf{N}^*(s+\Delta s)\end{aligned}$$

which basically consists in projecting previous normal and binormal vectors on the current orthogonal plane. The generalized cylinder is endowed with energy functional E, weighted sum of the internal energy E_{smooth} and the external region energy E_{data}:

$$E[\phi, \mathcal{R}] = \omega E_{\text{smooth}}[\phi, \mathcal{R}] + (1-\omega)E_{\text{data}}[\phi, \mathcal{R}] \qquad (2)$$

The user-provided coefficient ω, weighting the influence of E_{smooth} over E_{data}, controls the elastic properties of the deformable band. Since E depends both on ϕ and $\mathcal{R}$, the cylinder minimizing E should satisfy two coupled Euler-Lagrange

equations:

$$\frac{\delta E[\phi,\mathcal{R}]}{\delta\phi}=\mathbf{0} \quad \text{and} \quad \frac{\delta E[\phi,\mathcal{R}]}{\delta\mathcal{R}}=0 \tag{3}$$

where the variational derivatives of the energy with respect to the curve and radius vanish. To express the regularization term, we rely on the reasonable assumption that a smooth axis curve and a smoothly varying radius will yield a smooth surface:

$$E_{\text{smooth}}[\phi,\mathcal{R}]=\int_0^1 \|\phi_s\|\,ds+\int_0^1\int_0^{2\pi}\mathcal{R}_s^2+\mathcal{R}_v^2\,dvds$$

The first variations of the smoothness term are:

$$\frac{\delta E_{\text{smooth}}}{\delta\phi}=-\|\phi_s\|\,\kappa\mathbf{N} \qquad \frac{\delta E_{\text{smooth}}}{\delta\mathcal{R}}=-2\left(\mathcal{R}_{ss}+\mathcal{R}_{vv}\right)$$

where κ is the curvature of ϕ. Let R_{in} and R_{out} be the inner and outer regions bounded by Γ. Since the structure of interest should satisfy an intensity homogeneity criterion, the data term is as follows:

$$E_{\text{data}}[\phi,\mathcal{R}]=\int_{R_{\text{in}}} g_{\text{in}}(\mathbf{x})d\mathbf{x}+\int_{R_{\text{out}}} g_{\text{out}}(\mathbf{x})d\mathbf{x} \tag{4}$$

where region descriptors g_{in} and g_{out} increase with respect to inhomogeneity of the enhanced intensity. We use $g_{\text{in}}(\mathbf{x})=(I(\mathbf{x})-\mu_{\text{tree}})^2$ and $g_{\text{out}}(\mathbf{x})=(I(\mathbf{x})-\mu_{\text{out}})^2$, where μ_{tree} and μ_{out} are the average intensities inside and outside the entire tree structure, respectively. Relying on the divergence theorem to write volume integrals on R_{in} and R_{out} as surface integrals of Γ, calculus of variations is used to express the first variation of the data term with respect to radius:

$$\frac{\delta E_{\text{data}}}{\delta\mathcal{R}}=\mathcal{R}(1-\mathcal{R}\kappa\cos v)(g_{\text{in}}(\Gamma)-g_{\text{out}}(\Gamma))$$

The previous term is actually divided by $\mathcal{R}$ when implemented in the gradient descent, so that an increase of radius does not yield an increase in its variation. The cylinder is implemented as a polygonal line of n vertices $\mathbf{p}_i$, each vertex being endowed with m angular positions with associated radii $\mathcal{R}_{ij}$. The initial curve is provided by the minimal path approach described in section 3, whereas initial radii are set to a given constant $\mathcal{R}^{(0)}$. Regarding our implementation, it is not necessary to calculate the first variation of E_{data} with respect to the axis. Indeed, the axis should remain in the center of the tube, as in the symmetry-seeking model in [9]. Hence, vertex coordinates are computed as centroids of angular positions when all radii have been updated. This is summarized by the following scheme:

$$\begin{aligned}
\mathcal{R}_{ij}^{(t+1)}&=\mathcal{R}_{ij}^{(t)}-\Delta t\;\delta E/\delta\mathcal{R}|_{\mathcal{R}=\mathcal{R}_{ij}}\\
\mathbf{p}_i^{(t+1)}&=\mathbf{p}_i^{(t)}\\
&\quad+\frac{1}{m}\sum_{j=1}^{m}\mathcal{R}_{ij}^{(t+1)}\left(\cos\left(\frac{2\pi j}{m}\right)\mathbf{N}_i^{(t)}+\sin\left(\frac{2\pi j}{m}\right)\mathbf{B}_i^{(t)}\right)\\
\mathbf{p}_i^{(t+2)}&=\mathbf{p}_i^{(t+1)}+\Delta t\;\delta E_{\text{smooth}}/\delta\phi|_{\phi=\mathbf{p}_i}
\end{aligned}$$

where $t+2$ actually corresponds to the smoothing step. To maintain sufficient vertex density, the curve is resampled after each deformation step, i.e. after gradient descent has been applied on all vertices. The evolution scheme is simultaneously applied on all cylinders in the tree.

5. REFINING SEGMENTATION WITH REGION-BASED LEVEL SETS

In order to allow comparison between the estimated region and ground truth, the tree volume should be voxelized into the image space. The conversion from real coordinates to integer voxel-wise coordinates may yield various inaccuracies, especially due to rounding errors. Hence, we perform a final refinement step using level-set based segmentation. We consider the level set function $\psi:\mathcal{D}\subset\mathbb{R}^3\rightarrow\mathbb{R}$ and its inner volume as $R_{\text{in}}=\{\mathbf{x}|\psi(\mathbf{x})\leq 0\}$. The voxelized tree is used as the initial inner volume. Function ψ deforms according to the evolution equation:

$$\frac{\partial\psi}{\partial t}=F(\mathbf{x})\,\|\nabla\psi(\mathbf{x})\|\;\;\forall\mathbf{x}\in\mathbb{R}^d \tag{5}$$

where speed function F is a weighted sum of smoothness and data terms:

$$F(\mathbf{x})=\omega F_{\text{smooth}}(\mathbf{x})+(1-\omega)F_{\text{data}}(\mathbf{x})$$

where coefficient ω controls the significance of the smoothness term. In the level set framework, regularization is usually based on curvature. In order to achieve a more diffuse regularization, we replace the curvature term with a Gaussian convolution, as in [10]. As regards the data term, one may note that vessels are brighter than neighboring structures like muscles and fat. With respect to intensity, they may be segmented using a straightforward region criterion. We consider the data term of the Chan-Vese model [6]:

$$E_{\text{data}}[\psi]=\int_{R_{\text{in}}(\psi)}(I(\mathbf{x})-k_{\text{in}})^2d\mathbf{x}+\int_{R_{\text{out}}(\psi)}(I(\mathbf{x})-k_{\text{out}})^2d\mathbf{x}$$

The data speed term is determined from the variational derivative of energy E_{data} with respect to ψ.

$$F_{\text{data}}(\mathbf{x})=\delta(\psi(\mathbf{x}))[-(I(\mathbf{x})-k_{\text{in}})^2+(I(\mathbf{x})-k_{\text{out}})^2]$$

Thanks to gradient descent, variables k_{in} and k_{out} are assigned to average intensities inside and outside the current region, respectively. For implementation purpose, we use a regularized version of the Dirac δ function, as in [6]. The level set function is updated according to the narrow band technique with a single pixel-wide band. One or two iterations are sufficient to achieve good surface fitting while preventing the region from propagating into undesirable vessels.

6. EXPERIMENTS

The deformable tree model was tested on 9 CTA images of the carotid bifurcation, where the Common Carotid Artery (CCA) branches off into the external (ECA) and internal (ICA) carotid arteries. Datasets were provided

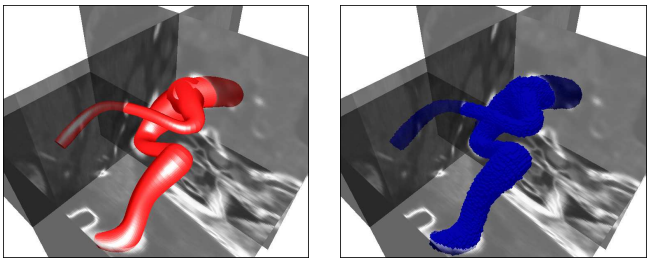

Fig. 4. Deformable tree (left) and corresponding voxelized volume (right) on CTA image of the carotid bifurcation

by the Biomedical Imaging Group from Erasmus MC in Rotterdam, for the carotid segmentation challenge [2], which was held in conjunction with MICCAI 2009 [11]. For each image, ground truth was available, so that segmentation accuracy could be quantified. We actually used the training database for testing, which makes sense as we do not perform any learning stage. Endpoints in each artery were part of provided data. We used the point in the CCA as the root for propagating the action map (see section 3), and the two other points as start locations for backtracking and building the initial paths. Hence, the deformable tree is only made up of a parent segment and two child segments (see fig. 4).

The initial radius $\mathcal{R}^{(0)}$ was typically set to 4 pixels. As regards regularization weight ω, both for the deformable tree and the implicit active surface, values ranging from 0.4 to 0.7 were sufficient to maintain smooth boundaries. The same set of parameters was suitable for all experiments. With a C++ implementation running on an Intel Core 2 Duo 2.2GHz PC (4Gb RAM), computational costs yielded by our approach are as follows: 8.3s for the construction of the initial tree, ≈ 15s for tree evolution and 4.5s for building and evolution of the refining level set. Quantitative segmentation results, with respect to ground truth data, are listed in table 1. We used the Dice region similarity measure as well as Hausdorff-based boundary similarity measures. The Hausdorff distance H_{max} and its modified version H_{mean} [12] respectively measure the maximal and mean euclidean distances from every voxel in the estimated surface to the closest one in the ground truth surface. We believe the reconstruction results to be promising, although we could not properly handle dataset 'challenge004', which was insufficiently contrasted to allow segmentation by the region-based criterion.

7. CONCLUSION AND FUTURE WORK

We described an explicit deformable tree, holding relationships between segments, for the extraction of branching structures. Deformation of the entire tree was performed by evolving generalized cylinders towards a minimum of an energy functional. Future work will focus on the formulation of local region terms handling intensity variations along branches, which we believe to be valuable for extracting thin and low-contrasted vessels. We may also consider automatic selection of initial segment endpoints, which could be done by studying particular differential quantities on the action map.

[2] See the web page of the challenge at `http://cls2009.bigr.nl/`

Data	Dice index (%)	H_{mean}	H_{max}
challenge000	94.9	0.437	7.071
challenge001	86.1	1.301	9.000
challenge002	90.1	0.849	3.606
challenge003	91.4	0.840	7.280
challenge004	X	X	X
challenge005	91.7	0.896	6.708
challenge006	92.3	0.663	6.708
challenge007	92.5	0.982	3.606
challenge008	94.6	0.536	5.831

Table 1. Segmentation measures with respect to ground truth: Dice index (% units), modified Hausdorff distance (pixel units) and Hausdorff distance (pixel units). Average pixel size is 0.25mm

8. REFERENCES

[1] C. Kirbas and F. Quek, "A review of vessel extraction techniques and algorithms," *ACM Computing Surveys*, vol. 36, no. 2, pp. 81–121, 2004.

[2] M.A. Gülsün and H. Tek, "Robust vessel tree modeling," in *MICCAI*, New York, USA, 2008, vol. 5303 of *LNCS*, pp. 602–611, Springer.

[3] J. Lee, P. Beighley, E. Ritman, and N. Smith, "Automatic segmentation of 3D micro-CT coronary vascular images," *Medical Image Analysis*, vol. 11, no. 6, pp. 630–647, 2007.

[4] H. Li and A. Yezzi, "Vessels as 4-D curves: global minimal 4-D paths to extract 3-D tubular surfaces and centerlines," *IEEE Transactions on Medical Imaging*, vol. 26, no. 9, pp. 1213–1223, 2007.

[5] L. Cohen and R. Kimmel, "Global minimum for active contour models: a minimal path approach," *International Journal of Computer Vision*, vol. 24, no. 1, pp. 57–78, 1997.

[6] T. Chan and L. Vese, "Active contours without edges," *IEEE Transactions on Image Processing*, vol. 10, no. 2, pp. 266–277, 2001.

[7] T.E. O'Donnell, T. Boult, X. Fang, and A. Gupta, "The Extruded Generalized Cylinder: a deformable model for object recovery," in *CVPR*, Seattle, USA, 1994, pp. 174–181.

[8] P.J. Yim, J.J. Cebral, R. Mullick, H.B. Marcos, and P.L. Choyke, "Vessel surface reconstruction with a tubular deformable model," *IEEE Transactions on Medical Imaging*, vol. 20, no. 12, pp. 1411–1421, 2001.

[9] D. Terzopoulos, A. Witkin, and M. Kass, "Symmetry-seeking models and 3d object reconstruction," *International Journal of Computer Vision*, vol. 1, no. 3, pp. 211–221, 1987.

[10] J. Mille, "Narrow band region-based active contours and surfaces for 2D and 3D segmentation," *Computer Vision and Image Understanding*, vol. 113, no. 9, pp. 946–965, 2009.

[11] K. Hameeteman, M. Freiman, M.A Zuluaga, L. Joskowicz, S. Rozie, M.J. Van Gils, L. Van den Borne, J. Sosna, P. Berman, N. Cohen, P. Douek, I. Sanchez, M. Aissat, A. Van der Lugt, G.P. Krestin, W.J. Niessen, and T. Van Walsum, "Carotid lumen segmentation and stenosis grading challenge," *The MIDAS Journal*, 2009.

[12] M-P. Dubuisson and A.K. Jain, "A modified Hausdorff distance for object matching," in *ICPR*, Jerusalem, Israel, 1994, pp. 566–568.